Hindawi Publishing Corporation
Journal of Nanomaterials
Volume 2016, Article ID 5208027, 10 pages
http://dx.doi.org/10.1155/2016/5208027

Research Article

The Pore Confinement Effect of FDU-12 Mesochannels on MoS_2 Active Phases and Their Hydrodesulfurization Performance

Cong Liu, Pei Yuan, and Chunsheng Cui

State Key Laboratory of Heavy Oil Processing, China University of Petroleum, Beijing 102249, China

Correspondence should be addressed to Pei Yuan; yuanpei@cup.edu.cn

Received 20 January 2016; Accepted 21 March 2016

Academic Editor: Reza Kharaghani

FDU-12 silica with highly ordered face-centered cubic mesoporous structure is developed as support to prepare Mo/FDU-12 catalysts for hydrodesulfurization (HDS) of dibenzothiophene (DBT). A series of Mo/FDU-12 catalysts are synthesized by using incipient wetness impregnation method with different MoO_3 loadings (6, 8, 10, 12, and 15 wt.%). The objective of this work is to explore the pore confinement effect of FDU-12 mesochannels on the MoS_2 morphology with various metal loadings. It is found that, as increasing MoO_3 loadings from 6 to 15 wt.%, the MoS_2 nanocrystallites transform from monolayer to multilayer and the morphology changes from straight layered to curved and then to ring-like and finally to spherical-like morphology due to the restriction of cage-like pore channels of FDU-12 support. The HDS results show that the catalytic activity increases first and then decreases with the best HDS performance at the MoO_3 loading of 10 wt.%. In addition, we compared the HDS activity of Mo catalyst supported on FDU-12 with that on the commercial γ-Al_2O_3 and SBA-15; the result exhibits that FDU-12 is superior to the other two supports due to its large pore size and ordered three-dimensional open pore channels.

1. Introduction

Ordered mesoporous materials with high surface area, large pore volume, ordered pore structure, and good thermal and mechanical stabilities have a broad range of applications in catalysis, adsorption, energy storage, and nanodevices due to their unique physical and chemical properties [1–4]. In general, the ordered mesostructures can be classified as two-dimensional (2D) and three-dimensional (3D) architecture according to the pore symmetry. The typical 2D mesoporous materials are SBA-15, MCM-41, and so forth [5, 6] and the 3D mesoporous materials usually include MCM-48, SBA-16, KIT-6, and FDU-12 [7, 8], whose property is considered to be superior to the former because the 3D channel is favorable for the mass transfer and diffusion of guest molecules. The mesoporous materials usually act as host to support the guest species or behave as a nanoreactor to provide a space for reaction, which are widely used in catalysis. When the active phase precursor is incorporated into the pores of the support, it can be inevitably restricted by the pore size and pore structure and, therefore, it is interesting to explore the pore confinement effect on the active phases.

One of the main applications of the mesoporous materials in catalysis field is as catalyst supports for hydrodesulfurization (HDS). HDS is considered to be the most effective method to bring down the sulfur content in fuels and produce ultra-low-sulfur clean fuels to fit the more and more stringent environmental policy [9, 10]. Among different materials recently as supports for HDS catalysts, the mesoporous silica materials with ordered pore structures such as SBA-15, MCM-41, and KIT-6 have attracted widespread attention [11–15]. FDU-12 is a kind of 3D material with a face-centered cubic (*Fm-3m*) symmetry and its particular property of highly open channel networks makes it possible for faster diffusion of reactants and products during the reaction without pore blockage as happened in MCM-41 and SBA-15 with linear pore channel structure [13]. But unfortunately, to the best of our knowledge, there is no report to investigate the pore confinement effect of the cage-like pore structure of FDU-12 on the active phases with the increase of metal loadings and further on the variation of HDS activity.

Herein, we apply the 3D cubic cage-like mesostructured FDU-12 as the support to prepare a series of Mo/FDU-12

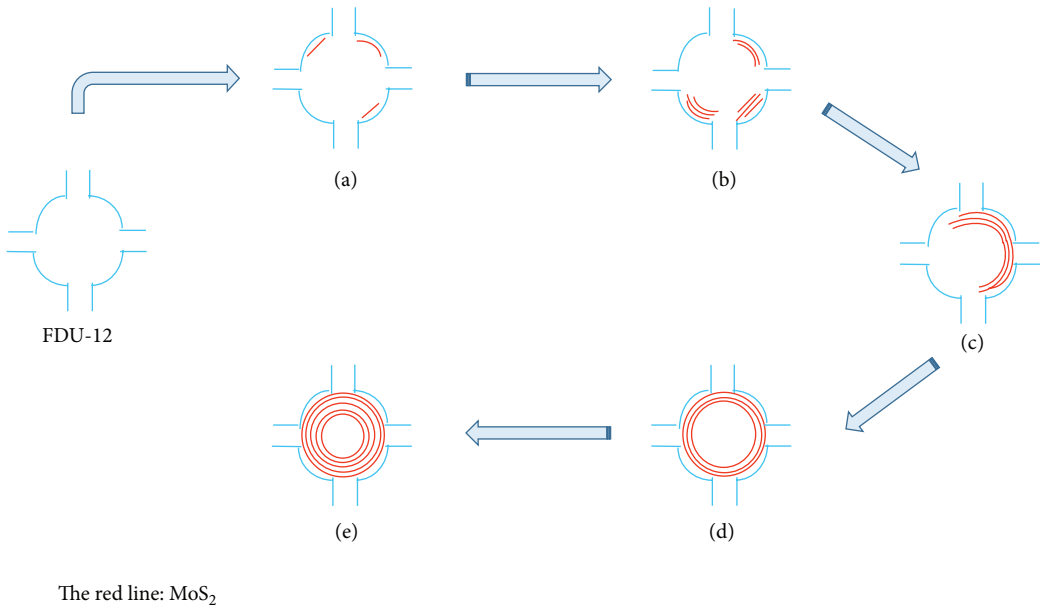

Scheme 1: The schematic diagram to illustrate the change of the morphology of MoS_2 active phases with different MoO_3 loadings supported on FDU-12.

catalysts with different MoO_3 loadings (6–15 wt.%) in order to systematically explore the pore confinement effect on the MoS_2 active phases and the HDS performance. The results show that the morphology of MoS_2 changes from straight layered to curved and then to ring-like and spherical-like morphology as increasing MoO_3 contents (Scheme 1) owing to the restriction of cage-like pore channels of FDU-12 support and the best HDS activity is found at MoO_3 loading of 10 wt.% with curved active phases. Moreover, the comparison of HDS activity is done with commercial γ-Al_2O_3 and SBA-15 supported catalysts, demonstrating the importance of the pore size and pore structure of catalyst support and highlighting the efficacy of FDU-12.

2. Experimental

2.1. Chemicals. All the chemicals were of analytical grade and used as received without further purification. Triblock copolymer poly(ethylene oxide)-poly(propylene oxide)-poly(ethylene oxide) F127 ($PEO_{106}PPO_{70}PEO_{106}$, M_W = 12600), tetraethyl orthosilicate (TEOS), 1,3,5-trimethylbenzene (TMB), potassium chloride (KCl), hydrochloric acid (HCl), and ammonium molybdate tetrahydrate were purchased from Aldrich. Dibenzothiophene (DBT) was purchased from Adamas-beta.

2.2. The Preparation of FDU-12 Support and Mo(x)/FDU-12 Catalysts. Mesoporous structured pure FDU-12 silica was synthesized according to the literature [8] using nonionic block copolymer F127 as template and TMB together with KCl as additives. In a typical synthesis, 2.0 g of F127 and 10.0 g of KCl were completely dissolved in 2 M HCl (120 mL) at 15°C, then 2.4 g of TMB was added, and the mixture was stirred at 15°C for 6 h, and next 8.32 g of TEOS was added to the above mixture. After stirring for 24 h at 15°C, the mixtures were directly transferred into an autoclave for hydrothermal treatment at 150°C for 24 h. The solid product was collected by filtration, washed with water, dried, and then calcined at 550°C for 5 h to remove the templates.

Mo catalysts supported on FDU-12 were prepared by incipient wetness impregnation method reported elsewhere by using appropriate concentration of ammonium molybdate tetrahydrate as Mo source. The MoO_3 loadings of the catalysts were 6, 8, 10, 12, and 15 wt.%, respectively. After impregnation, all the catalysts were dried at 80°C for 12 h and calcined at 500°C for 4 h in static air atmosphere denoted by Mo(x)/FDU-12, in which x represents the MoO_3 content. For comparison, γ-Al_2O_3 and mesoporous SBA-15 supported catalysts with MoO_3 content of 10 wt.% were prepared according to the same loading method.

2.3. Catalyst Characterization. Small angle X-ray scattering (SAXS) profiles of the support were obtained from Bruker NanoSTAR with a 2D detector and X-ray beam pinhole collimated (40 kV, 30 mA). N_2 adsorption-desorption measurements of the support and corresponding catalysts were performed on a Micromeritics ASAP 2002 instrument (USA). The specific surface areas were calculated using the Brunauer-Emmett-Teller (BET) method and the pore size distributions were obtained using the Barrett-Joyner-Halenda (BJH) method [16]. The samples to be measured were firstly degassed in the preparation station at 180°C and a vacuum of 10^{-5} Torr for 15 h and then switched to the analysis station for adsorption-desorption experiment at −196°C. Powder X-ray diffraction (XRD) experiments were performed using a Philips X'Pert diffractometer equipped with Cu Kα radiation (wavelength 1.5406 Å). XRD patterns were collected with the 2θ range between 8° and 70°, a step size of 2°, and a counting

time of 60 s per step. UV-vis diffuse reflection spectroscopy (UV-vis DRS) experiments were performed on a Hitachi U-4100 UV-vis spectrophotometer with the integration sphere diffuse reflectance attachment. The powder samples were loaded into a transparent quartz cell and were measured in the region of 200–600 nm under ambient conditions. The standard support reflectance was used as the baseline for the corresponding catalyst measurement.

The morphological features of the catalysts were obtained from high resolution transmission electron microscopy (HRTEM) with a Tecnai F20 at 200 kV. The powder samples were grounded smoothly in an agate mortar and dispersed in ethanol in an ultrasonic bath for several minutes. X-ray photoelectron spectroscopy (XPS) measurements of the sulfided catalysts were performed on a VG ESCA Lab 250 spectrometer using AlKα radiation. To quantify the contents of Mo^{4+}, Mo^{5+}, and Mo^{6+} species, the XPS spectra obtained were fitted using XPSPEAK software (version 4.1). A Shirley background was applied and the Mo 3d spectra were deconvoluted by fitting the experimental spectra to a mixed Gaussian-Lorentzian function.

2.4. Catalytic Activity. The HDS activity tests were performed in a continuous fixed bed reactor with 0.5 g catalyst. Before the catalytic activity testing, the catalysts were sulfided with a mixture of 3 wt.% CS_2 and cyclohexane at 360°C for 4 h, under 4.0 MPa H_2 pressure. After sulfidation, 1 wt.% DBT in heptanes used as a model compound was fed to the reactor under the conditions of reaction temperature of 360°C, H_2/oil of 300, and weight hourly space velocity (WHSV) of 13 h^{-1}. After evaluation, the reaction products were collected and the sulfur content of products was analyzed by a WK-2C type microcoulomb meter.

Assuming a pseudo-first-order reaction for HDS of DBT, the activity of the catalysts can be expressed by [17]

$$k_{\mathrm{HDS}} = \frac{F}{m} \ln\left(\frac{1}{1-\tau}\right), \quad (1)$$

where F is the feeding rate of the reactant in mol s^{-1}, m is the catalyst mass in grams, τ is the total conversion of DBT, and k_{HDS} is the rate constant of HDS in mol g^{-1} s^{-1}.

3. Results and Discussion

3.1. Characterization of FDU-12 Support and Mo(x)/FDU-12 Catalysts in Oxidic State. The SAXS pattern of the pure silica FDU-12 hydrothermally treated at 150°C is shown in Figure 1. It exhibits six characteristic peaks, which should be assigned to the (111), (220), (311), (420), (333), and (531) reflections of a face-centered cubic structure [8], indicating the successful synthesis of highly ordered FDU-12 mesoporous silica.

Figure 2(a) presents the N_2 adsorption-desorption isotherms of FDU-12 support and Mo(x)/FDU-12 catalysts and they all exhibit type IV isotherm with H2 hysteresis loop demonstrating the cage-like mesostructure. The shape of the isotherm and the hysteresis loop does not suffer evident changes after the incorporation of Mo species. The pore size distribution curves calculated from the adsorption branch

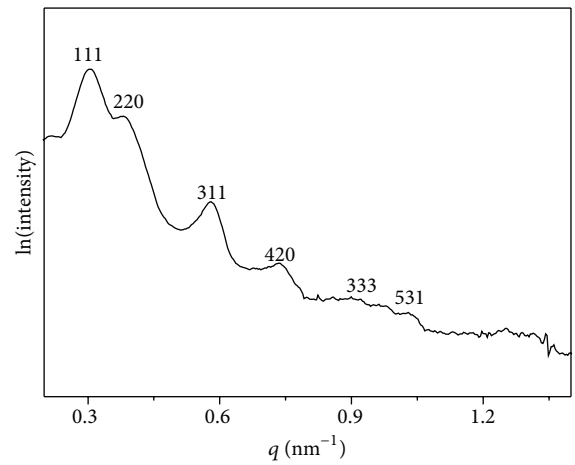

Figure 1: SAXS pattern of FDU-12 support.

Table 1: Textural and structural characteristics of FDU-12 support, Mo(x)/FDU-12, Mo(10)/SBA-15, and Mo(10)/γ-Al_2O_3 catalysts.

Sample	S_{BET} (m^2/g)[a]	V_t (cm^3/g)[b]	D_p (nm)
FDU-12	346.4	0.90	17.4[c] (8.7[d])
Mo(6)/FDU-12	325.5	0.87	17.2 (8.6)
Mo(8)/FDU-12	316.8	0.82	17.2 (8.6)
Mo(10)/FDU-12	310.1	0.79	17.2 (8.5)
Mo(12)/FDU-12	296.3	0.76	17.1 (8.5)
Mo(15)/FDU-12	268.9	0.68	16.8 (8.4)
Mo(10)/SBA-15	623.5	0.81	7.1
Mo(10)/γ-Al_2O_3	226.1	0.35	5.9

Note: [a]specific surface area calculated by BET method, [b]pore volume, [c]pore diameters calculated from the adsorption branch, and [d]window sizes obtained from the desorption branch by using the BJH method.

(Figure 2(b)) and desorption branch (Figure 2(c)) show a monomodal distribution with the pore diameter (cage size) centered at ca. 17 nm and window size centered at ca. 8.5 nm, respectively, and it is clear that, after the incorporation of Mo species, both of the cage and window size remain essentially unchanged.

The textural and structural characteristics (the specific surface area S_{BET}, total pore volume V_t, and pore diameter D_p) of the FDU-12 support and corresponding catalysts obtained by N_2 sorption results are summarized in Table 1. FDU-12 support has a BET surface area of 346.4 m^2/g and total pore volume of 0.90 cm^3/g and Mo(6)/FDU-12 catalyst only has a slight drop in surface area and pore volume since an increase in the sample's density after the incorporation of Mo species. However, this drop gradually becomes more apparent with the increase of MoO_3 contents, especially for Mo(15)/FDU-12 catalyst because the excess loadings may lead to the agglomeration of Mo species, partially blocking the pores of FDU-12.

More information about the aggregation and coordination state of the oxidic Mo species in Mo(x)/FDU-12 catalysts was provided by XRD and UV-vis DRS. The powder XRD patterns (Figure 3(a)) all exhibit a very broad peak at around

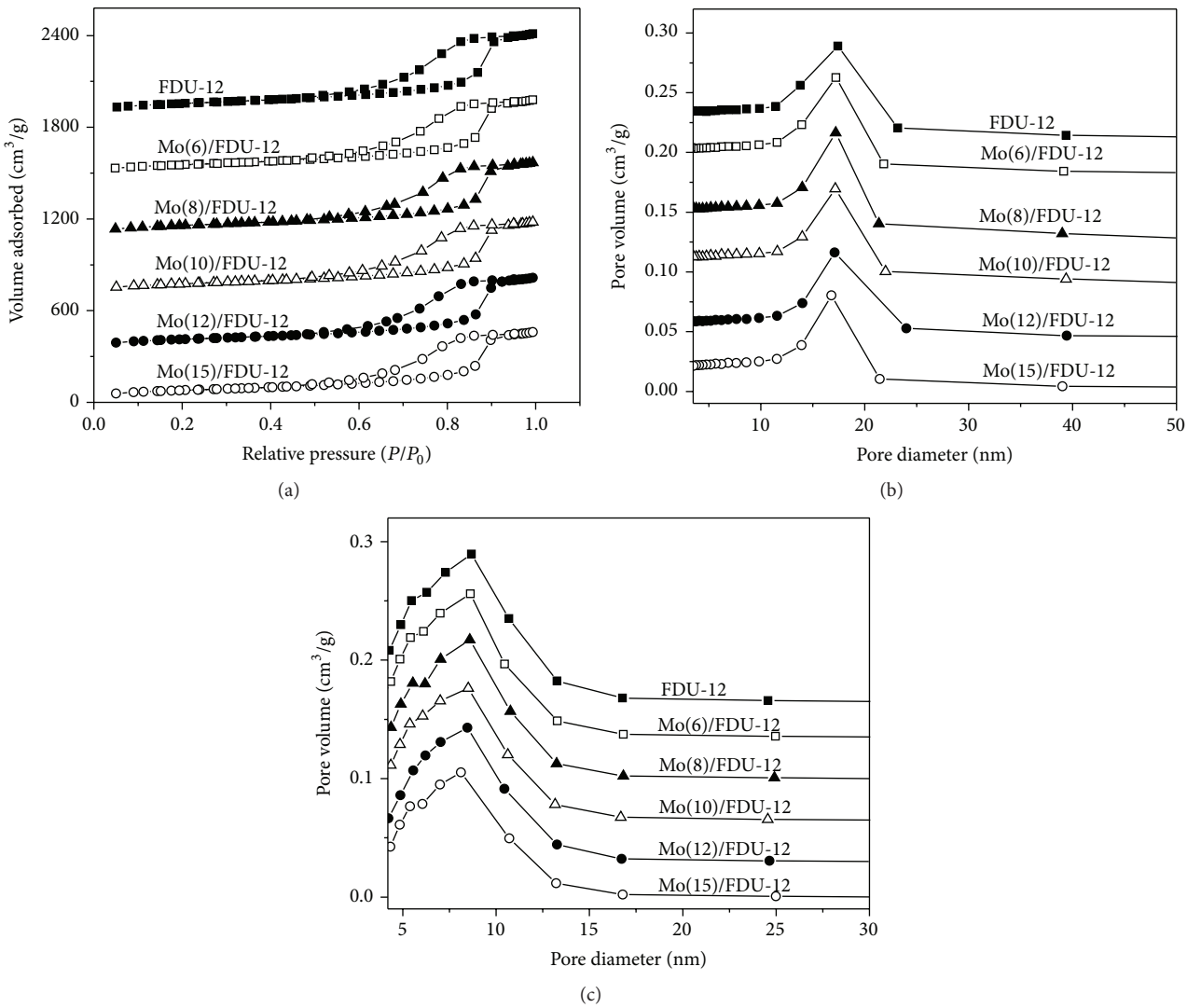

FIGURE 2: N_2 adsorption-desorption isotherms (a) and pore size distribution curves calculated from the adsorption branch (b) and desorption branch (c) of FDU-12 support and Mo(x)/FDU-12 catalysts.

$2\theta = 24^\circ$, typical of amorphous silica. At lower MoO_3 loadings (6, 8, and 10 wt.%), there is no signal of any crystalline phase indicating the well-dispersed Mo species over the support. With the increase of MoO_3 loadings, the signals of MoO_3 crystallite phase are detected on Mo(12)/FDU-12 catalyst, but the signal strength is very weak. Nevertheless, with respect to Mo(15)/FDU-12 catalyst, there are four characteristic peaks that can be clearly observed at 2θ = 12.7, 23.4, 25.7, 27.4°, which are attributed to the bulk MoO_3 crystallite phase (PDF 05-0508). The excess loadings may result in the aggregation of metal oxides on the pure silica support due to the weak support-metal interaction and it will form large particles after the high-temperature calcination, which are hard to be sulfided and thereby unfavorable for the catalytic activity.

Figure 3(b) shows DRS spectra of the Mo(x)/FDU-12 catalysts and the absorption band in the spectra corresponds to the ligand-to-metal charge transfer (LMCT) $O^{2-} \rightarrow Mo^{6+}$. It is common knowledge that the position of this LMCT absorption band depends intensely on the local symmetry around the Mo^{6+} species and their aggregation state [18]. As reported elsewhere [19], the isolated molybdate species in tetrahedral coordination (Td) show a typical absorption band at about 250 nm; nevertheless the signal of polymolybdate species in octahedral coordination (Oh) is examined at the 280–330 nm range and its position is influenced by the aggregate size. Besides, both types of Mo^{6+} species exhibit the second strong absorption band at about 220 nm. As can be seen from the spectra, a mixture of Mo species in tetrahedral and octahedral coordination is present in all Mo(x)/FDU-12 catalysts, but the Mo absorption edges produce a slight red shift with increasing the MoO_3 loadings, indicating the occurrence of the large MoO_3 clusters, which is consistent with a decrease in the dispersion of Mo species detected by XRD (Figure 3(a)).

3.2. Characterizations of Mo(x)/FDU-12 Catalysts in Sulfided State. Figure 4 displays the HRTEM images of the five Mo/FDU-12 catalysts with different MoO_3 loadings to obtain more information about the morphology and dispersion of

Table 2: The mole atomic ratio of S/Mo, sulfidation degree ($Mo_{sulfidation}$), HDS ratio, and rate constant (k_{HDS}) of sulfided Mo(x)/FDU-12 catalysts.

Catalysts	S/Mo	$Mo_{sulfidation}$	HDS ratio (%)	k_{HDS} (10^{-7} mol g^{-1} s^{-1})
Mo(6)/FDU-12	1.3	43.8	70.6	0.22
Mo(8)/FDU-12	1.7	60.2	83.8	0.36
Mo(10)/FDU-12	2.1	69.0	91.7	0.43
Mo(12)/FDU-12	1.5	51.6	76.1	0.31
Mo(15)/FDU-12	1.0	37.5	60.4	0.16
Mo(10)/SBA-15	—	—	86.0	0.38
Mo(10)/γ-Al_2O_3	—	—	80.2	0.34

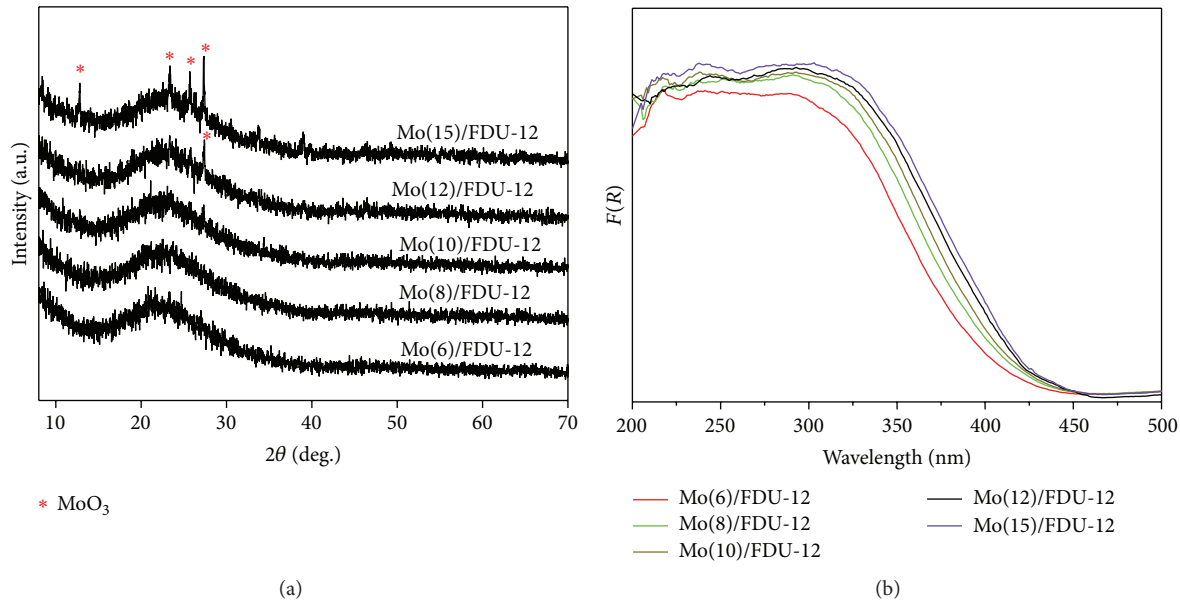

Figure 3: XRD patterns (a) and DRS spectra (b) of FDU-12 support and Mo(x)/FDU-12 catalysts.

MoS_2 nanocrystallites over the support. It can be clearly seen that Mo(6)/FDU-12 displays mostly straight monolayered MoS_2 nanocrystallines with short length (Figure 4(a)) and Mo(8)/FDU-12 catalyst shows straight multilayered MoS_2 active phases (Figure 4(b)), which are similar to the case in SBA-15 supported catalysts [20]. While when the MoO_3 loading increases to 10 wt.%, slightly larger and highly stacked MoS_2 particles are formed, more importantly, the morphology of MoS_2 (Figure 4(c)) which is restricted by the cage-like pores of FDU-12 support is visible bended. Further increasing the metal loadings, the curved MoS_2 crystallites keep on growing along with the eyeball until they form a closed ring-like structure for Mo(12)/FDU-12 catalyst (Figure 4(d)), which is quite differentiated with 2D pore channels of SBA-15 support. When the MoO_3 content is up to 15 wt.%, a much more stacked arrangement of MoS_2 crystallites is observed and the cages of FDU-12 support are almost fully filled by the spherical-like layered MoS_2, suggesting the growth of active phases is actually along the pore walls (Figure 4(e)). It can be concluded that, with the increase of MoO_3 loadings from 6 to 15 wt.%, the morphology of MoS_2 active phases changes from straight layered to curved and then to ring-like and spherical-like morphology, revealing that MoS_2 morphology is strongly affected by the pore structure of support.

The Mo 3d XPS spectra of the sulfided Mo catalysts supported on FDU-12 were measured and employed to determine the state of Mo species after sulfidation (Figure 5). The binding energies of the Mo $3d_{5/2}$ and Mo $3d_{3/2}$ levels for Mo^{4+} (MoS_2) are about 229.1 and 232.0 eV, respectively, those for Mo^{5+} (MoO_xS_y) are about 230.5 and 233.8 eV, and those for Mo^{6+} (MoO_3) are about 232.8 and 236.0 eV [21, 22], and the binding energy at about 226.5 eV is ascribed to the S 2s level. The sulfidation degree of Mo species, $Mo_{sulfidation}$, is expressed as $Mo^{4+}/(Mo^{4+} + Mo^{5+} + Mo^{6+})$ ratio and the corresponding results are calculated in Table 2. It is shown that the sulfidation degree of the Mo catalysts increases with the increase of metal loadings and reaches the highest value (69.0%) for Mo(10)/FDU-12 catalyst, due to the formation of well-dispersed MoS_2 nanoparticles with suitable stacking layer numbers. However, with the further increase of MoO_3 loadings, the $Mo_{sulfidation}$ decreases and downgrades to the lowest value (37.5%) for Mo(15)/FDU-12 catalyst because of

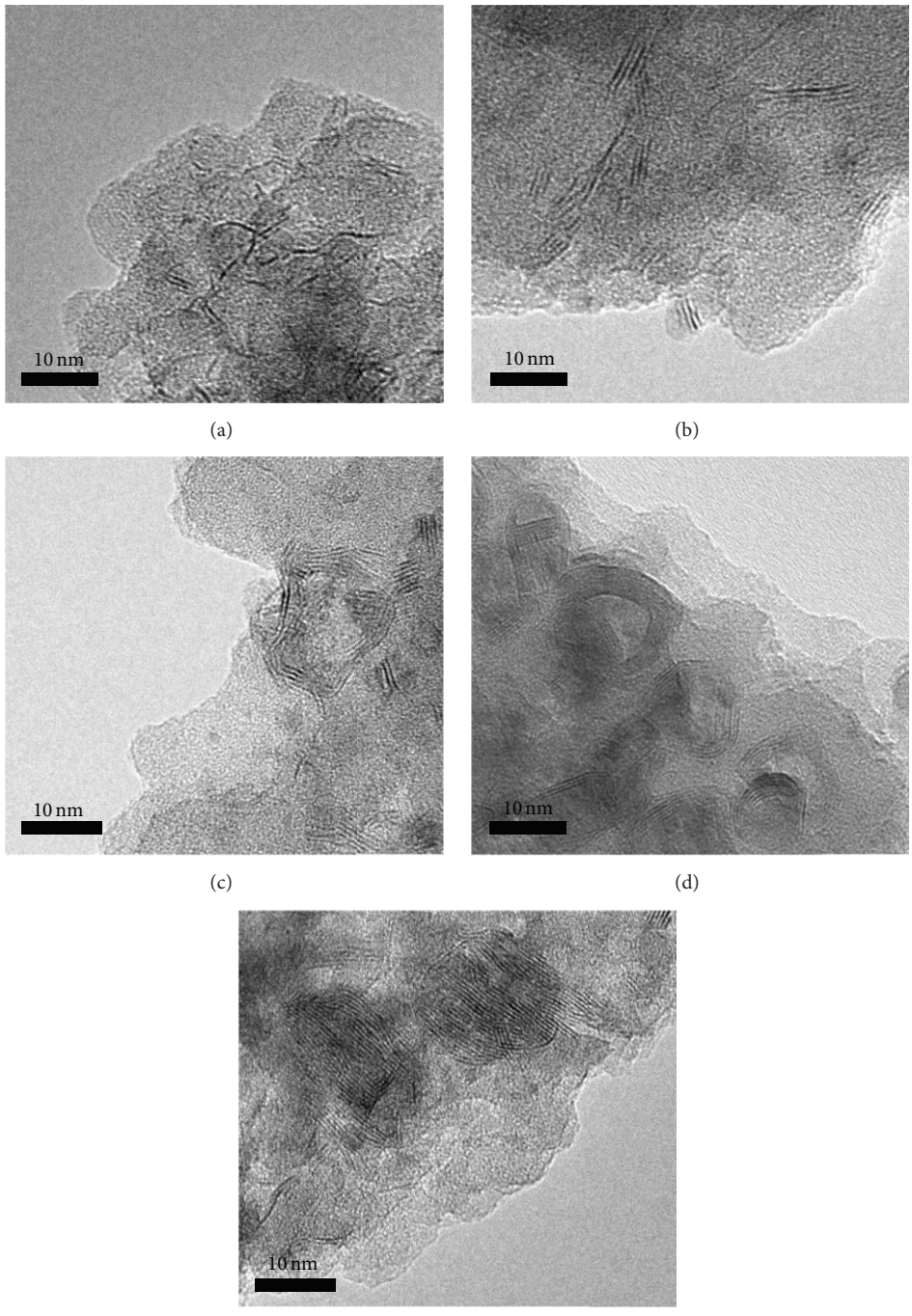

Figure 4: HRTEM images of the sulfided catalysts: (a) Mo(6)/FDU-12, (b) Mo(8)/FDU-12, (c) Mo(10)/FDU-12, (d) Mo(12)/FDU-12, and (e) Mo(15)/FDU-12.

the existence of bulk MoO_3 crystallites which are hard to be sulfided. The surface S/Mo atomic ratios of Mo(x)/FDU-12 catalysts were also determined by XPS and the results are given in Table 2. The S/Mo mole atomic ratio presents a similar trend which is in good accordance with the results of sulfidation degree.

3.3. HDS Catalytic Activity. HDS catalytic behaviors of Mo(x)/FDU-12 catalysts were evaluated in a continuously flowing tubular fixed bed microreactor by using DBT as a model compound which is a representative sulfur-containing compound for diesel fuel. By comparison, the values of the pseudo-first-order rate constant k_{HDS} which is present

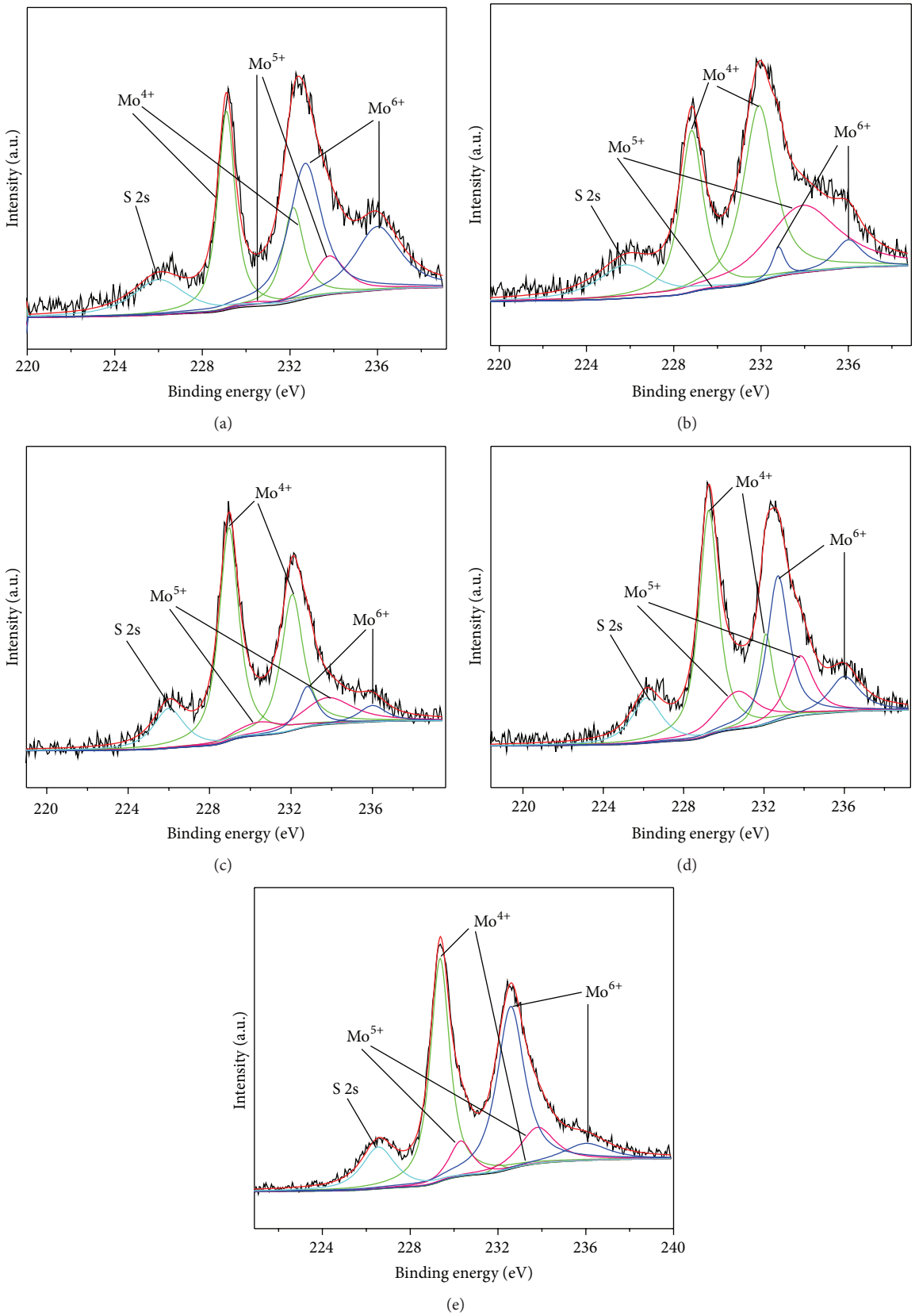

Figure 5: Mo 3d XPS spectra of the sulfided catalysts: (a) Mo(6)/FDU-12, (b) Mo(8)/FDU-12, (c) Mo(10)/FDU-12, (d) Mo(12)/FDU-12, and (e) Mo(15)/FDU-12.

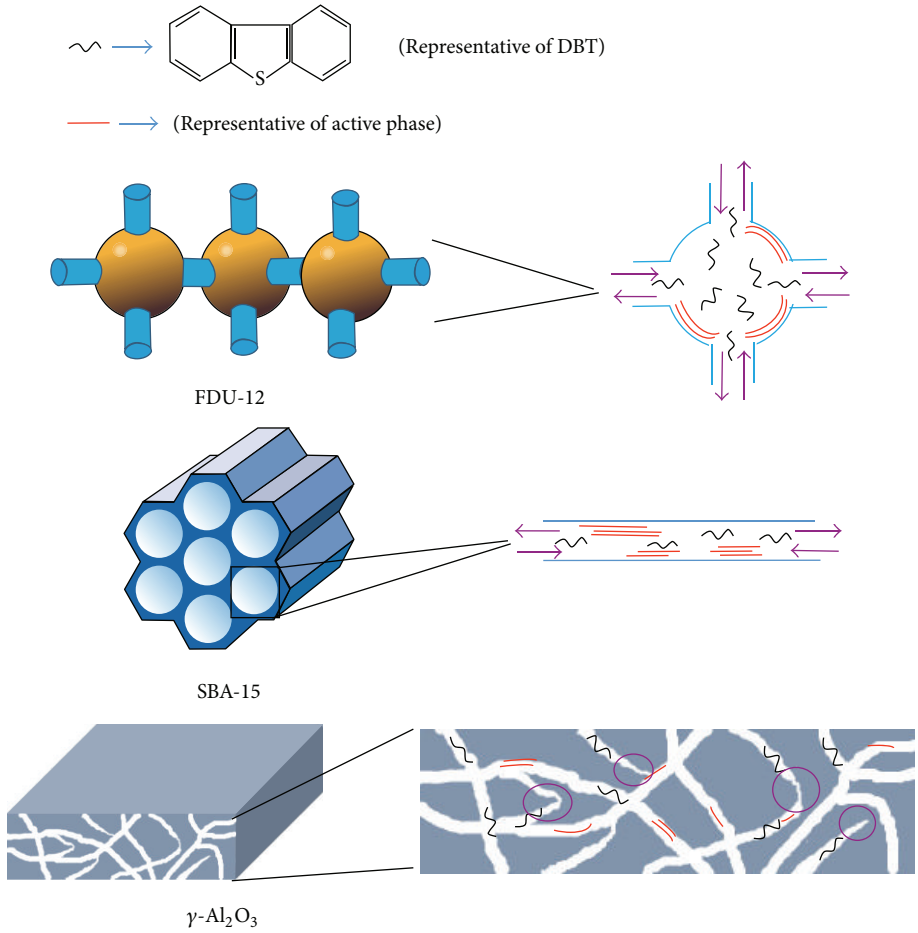

Scheme 2: The schematic diagram of DBT molecules diffusion in the pore of Mo(10)/FDU-12, Mo(10)/SBA-15, and Mo(10)/γ-Al_2O_3, respectively.

in a similar law for the five catalysts are summarized in Table 2. It is shown that the HDS activity of Mo(x)/FDU-12 catalysts increases from 70.6% to 91.7% and then decreases to 60.4% with the best HDS performance at MoO_3 loading of 10 wt.%. Mo(10)/FDU-12 catalyst possesses the highest k_{HDS} (0.42), which is about twice higher than Mo(6)/FDU-12 catalyst (k_{HDS} of 0.22) and almost three times better than Mo(15)/FDU-15 catalyst (k_{HDS} of 0.16). The low HDS ratio at low metal loadings is due to the limited active sites over the support and the monolayer morphology with low activity. Further increasing the MoO_3 loadings, the MoS_2 active phases become curved morphology with suitable stacking layers which has been reported to have more active sites than straight ones [23]; thus the catalyst exhibits the best HDS activity. However, when more Mo precursors enter into the cage-like pores of FDU-12, it happens to aggregate and forms spherical-like morphology because of the pore confinement effect, and such morphology leads to the dramatic decrease of the amounts of active sites and thus results in a poor HDS performance.

In addition, in order to reflect the superiority of three-dimensional mesostructure and explore the support effect, it is interesting to compare the catalytic activities of Mo/FDU-12 catalyst with using SBA-15 and γ-Al_2O_3 as supports at the same MoO_3 loading of 10 wt.%. SBA-15 has a two-dimensional mesostructure and γ-Al_2O_3 usually has irregular pore channels and nonuniform pore sizes and the textural properties of Mo(10)/SBA-15 and Mo(10)/γ-Al_2O_3 are given in Table 1. The results indicate that FDU-12 supported catalyst is more active (HDS ratio of 91.7%) than the other two catalysts with HDS ratio of 86.0% and 80.2%. It is well known that the restrictive diffusion factor, $F(\lambda)$, is usually used to describe the diffusion limitations [24]. $F(\lambda)$ value is inversely proportional to λ (λ represents the ratio of the molecular diameter to the pore diameter) and thus, for a fixed molecular diameter, the larger the pore diameter, the smaller the restrictive diffusion effect. The window size (which is the main factor to affect the molecular diffusion) of Mo(10)/FDU-12 and the pore size of Mo(10)/SBA-15 and Mo(10)/γ-Al_2O_3 are 8.5, 7.1, and 5.9 nm, respectively; thus the difference of $F(\lambda)$ value is quite small, especially for Mo(10)/FDU-12 and Mo(10)/SBA-15. Therefore, the better HDS performance for Mo(10)/FDU-12 should be attributed to its three-dimensional open structure which is more favorable for the molecules

diffusion in the pore channels to increase the accessibility to the active sites as demonstrated in Scheme 2.

4. Conclusion

In this study, cage-like mesostructured FDU-12 material was applied as support to synthesize a series of Mo/FDU-12 catalysts with different MoO_3 loadings in order to explore the pore confinement effect on active phases and the HDS activity. The dispersion and the morphology of MoS_2 vary with the increase of MoO_3 loadings. It is intriguing to note that due to the restriction of the cage-like pores of FDU-12 support, the layered MoS_2 crystallites transform from straight to slightly curved then to ring-like and finally to spherical-like morphology in the pores. For the HDS evaluation, Mo(10)/FDU-12 with the proper metal loading exhibits the highest HDS activity since the well-dispersed and curved MoS_2 nanoparticles with suitable stacking layer numbers expose more active sites. Furthermore, it is found that FDU-12 with 3D open pore structure and large pore size is more favorable for reactants diffusion and thus it shows to be superior as catalyst support compared with γ-Al_2O_3 and SBA-15.

Competing Interests

The authors declare that they have no competing interests.

Acknowledgments

This work was financially supported by the National Natural Science Foundation of China (Grants 21106182 and 21576290), the Research Fund for Public Welfare Project (201410015), and the Beijing Nova Program (Grant 2011106).

References

[1] M. E. Davis, "Ordered porous materials for emerging applications," *Nature*, vol. 417, pp. 813–821, 2002.

[2] A. Taguchi and F. Schüth, "Ordered mesoporous materials in catalysis," *Microporous and Mesoporous Materials*, vol. 77, no. 1, pp. 1–45, 2005.

[3] M. Hartmann, "Ordered mesoporous materials for bioadsorption and biocatalysis," *Chemistry of Materials*, vol. 17, no. 18, pp. 4577–4593, 2005.

[4] Z. Wu and D. Zhao, "Ordered mesoporous materials as adsorbents," *Chemical Communications*, vol. 47, no. 12, pp. 3332–3338, 2011.

[5] D. Zhao, J. Feng, Q. Huo et al., "Triblock copolymer syntheses of mesoporous silica with periodic 50 to 300 angstrom pores," *Science*, vol. 279, no. 5350, pp. 548–552, 1998.

[6] C. T. Kresge, M. E. Leonowicz, W. J. Roth, J. C. Vartuli, and J. S. Beck, "Ordered mesoporous molecular sieves synthesized by a liquid-crystal template mechanism," *Nature*, vol. 359, no. 6397, pp. 710–712, 1992.

[7] Q. Huo, R. Leon, P. M. Petroff, and G. D. Stucky, "Mesostructure design with gemini surfactants: supercage formation in a three-dimensional hexagonal array," *Science*, vol. 268, no. 5215, pp. 1324–1327, 1995.

[8] J. Fan, C. Yu, F. Gao et al., "Cubic mesoporous silica with large controllable entrance sizes and advanced adsorption properties," *Angewandte Chemie—International Edition*, vol. 42, no. 27, pp. 3146–3150, 2003.

[9] D. Czachowska-Kozłowska and M. Lewandowski, "New processes of deep hydrodesulfurization of diesel fuels," *Przemysl Chemiczny*, vol. 81, no. 9, pp. 577–582, 2002.

[10] A. Stanislaus, A. Marafi, and M. S. Rana, "Recent advances in the science and technology of ultra low sulfur diesel (ULSD) production," *Catalysis Today*, vol. 153, no. 1-2, pp. 1–68, 2010.

[11] D. Valencia and T. Klimova, "Citric acid loading for MoS_2-based catalysts supported on SBA-15. New catalytic materials with high hydrogenolysis ability in hydrodesulfurization," *Applied Catalysis B: Environmental*, vol. 129, pp. 137–145, 2013.

[12] P. Yuan, J. X. Liu, Y. T. Li et al., "Effect of pore diameter and structure of mesoporous sieve supported catalysts on hydrodesulfurization performance," *Chemical Engineering Science*, vol. 111, pp. 381–389, 2014.

[13] Z. Cao, A. Duan, Z. Zhao et al., "A simple two-step method to synthesize the well-ordered mesoporous composite Ti-FDU-12 and its application in the hydrodesulfurization of DBT and 4,6-DMDBT," *Journal of Materials Chemistry A*, vol. 2, no. 46, pp. 19738–19749, 2014.

[14] M. J. B. Souza, A. M. Garrido Pedrosa, J. A. Cecilia, A. M. Gil-Mora, and E. Rodríguez-Castellón, "Hydrodesulfurization of dibenzothiophene over PtMo/MCM-48 catalysts," *Catalysis Communications*, vol. 69, pp. 217–222, 2015.

[15] K. Soni, B. S. Rana, A. K. Sinha et al., "3-D ordered mesoporous KIT-6 support for effective hydrodesulfurization catalysts," *Applied Catalysis B: Environmental*, vol. 90, no. 1-2, pp. 55–63, 2009.

[16] P. Yuan, L. Tan, D. Pan et al., "A systematic study of long-range ordered 3D-SBA-15 materials by electron tomography," *New Journal of Chemistry*, vol. 35, no. 11, pp. 2456–2461, 2011.

[17] G. Berhault, M. Perez De la Rosa, A. Mehta, M. J. Yácaman, and R. R. Chianelli, "The single-layered morphology of supported MoS_2-based catalysts—the role of the cobalt promoter and its effects in the hydrodesulfurization of dibenzothiophene," *Applied Catalysis A: General*, vol. 345, no. 1, pp. 80–88, 2008.

[18] R. S. Weber, "Effect of local structure on the UV-visible absorption edges of molybdenum oxide clusters and supported molybdenum oxides," *Journal of Catalysis*, vol. 151, no. 2, pp. 470–474, 1995.

[19] R. L. Cordero and A. L. Agudo, "Effect of water extraction on the surface properties of Mo/Al_2O_3 and $NiMo/Al_2O_3$ hydrotreating catalysts," *Applied Catalysis A: General*, vol. 202, no. 1, pp. 23–35, 2000.

[20] O. Y. Gutiérrez and T. Klimova, "Effect of the support on the high activity of the (Ni) Mo/ZrO_2–SBA-15 catalyst in the simultaneous hydrodesulfurization of DBT and 4, 6-DMDBT," *Journal of Catalysis*, vol. 281, no. 1, pp. 50–62, 2011.

[21] T. Weber, J. C. Muijsers, J. H. M. C. Van Wolput, C. P. J. Verhagen, and J. W. Niemantsverdriet, "Basic reaction steps in the sulfidation of crystalline MoO_3 to MoS_2, as studied by X-ray photoelectron and infrared emission spectroscopy," *The Journal of Physical Chemistry*, vol. 100, no. 33, pp. 14144–14150, 1996.

[22] B. Liu, Y. Chai, Y. Li, A. Wang, Y. Liu, and C. Liu, "Effect of sulfidation atmosphere on the performance of the $CoMo/\gamma$-Al_2O_3 catalysts in hydrodesulfurization of FCC gasoline," *Applied Catalysis A: General*, vol. 471, pp. 70–79, 2014.

[23] R. Huirache-Acuña, B. Pawelec, E. Rivera-Muñoz, R. Nava, J. Espino, and J. L. G. Fierro, "Comparison of the morphology and HDS activity of ternary Co-Mo-W catalysts supported on P-modified SBA-15 and SBA-16 substrates," *Applied Catalysis B: Environmental*, vol. 92, no. 1-2, pp. 168–184, 2009.

[24] M.-C. Tsai, Y.-W. Chen, and C. Li, "Restrictive diffusion under hydrotreating reactions of heavy residue oils in a trickle bed reactor," *Industrial and Engineering Chemistry Research*, vol. 32, no. 8, pp. 1603–1609, 1993.